RNA Stores Tau Reversibly in Complex Coacervates

Xuemei Zhang[1,4], Neil A. Eschmann[2], Yanxian Lin[3], Hongjun Zhou[1,4], Jennifer Rauch[1,4], Israel Hernandez[1,4], Elmer Guzman[1,4], Kenneth S. Kosik[*,1,4], Songi Han[*,2,3,5]

[1] Molecular, Cell and Developmental Biology, University of California Santa Barbara, Santa Barbara, CA 93106, USA.

[2] Department of Chemistry and Biochemistry, University of California Santa Barbara, Santa Barbara, CA 93106, USA.

[3] Biomolecular Science and Engineering, University of California Santa Barbara, Santa Barbara, CA 93106, USA.

[4] Neuroscience Institute, University of California Santa Barbara, Santa Barbara, CA 93106, USA.

[5] Department of Chemical Engineering, University of California Santa Barbara, Santa Barbara, CA 93106, USA.

*Correspondence to: kenneth.kosik@lifesci.ucsb.edu; songi@chem.ucsb.edu

Competing interests

The authors declare no competing financial interests.

Contributions

K.S.K. and S.H. designed experiments; X.Z. did the PAR-iCLIP experiments, the *in vitro* RNA-protein binding assays; E.G. sequenced the DNA libraries; H.Z. performed bioinformatics

analysis; J.R. did ITC experiments; N.A.E., Y.L. and J.R. did the RNA-Tau *in vitro* droplet formation; N.A.E. did EPR and DEER experiments; I.H. did sarkosyl fractionation; Y.L. and H.Z., contributed to manuscript preparation; X.Z., K.S.K. and S.H. wrote the manuscript.

Abstract

Non-membrane bound organelles that behave like liquid droplets are widespread among eukaryotic cells. Their dysregulation appears to be a critical step in several neurodegenerative conditions. Here we report that Tau protein, the primary constituent of Alzheimer neurofibrillary tangles, can form liquid droplets and therefore has the necessary biophysical properties to undergo a liquid-liquid phase separation (LLPS) in cells. Consonant with the factors that induce LLPS, Tau is an intrinsically disordered protein that electrostatically complexes with RNA to form droplets that can be tuned by salt concentration and temperature and exhibit low interfacial tension. Uniquely, the pool of RNAs to which Tau binds in living cells are tRNAs. This phase state of Tau is held in 1:1 charge balance across large blocks of the protein and the nucleic acid and forms optimal complexes at multiple RNA:Tau mass ratios. These features define a complex co-acervate in which undergo free diffusion in their interior, despite the high concentration of protein, and rapid exchange with their exterior environment. Counter to most closely packed protein assemblies, the condensed phase state of Tau is not associated with changes in local Tau conformations as verified by distance measurements across a pair of spin labels by pulsed dipolar spectroscopy. In contrast, fibrillar states of Tau are accompanied by large changes in local Tau conformations. Importantly, prolonged residency within a droplet results in the emergence of detectable beta-structure by thioflavin labeling, suggesting that the droplet state can incubate Tau and pre-dispose it toward beta sheet structures typical of insoluble Tau fibrils.

44

45 ## Introduction

46 Inclusions consisting of the Tau protein occur in many neurological conditions with
47 Alzheimer's disease the most prominent among them. Normally, Tau is in a kinetic equilibrium
48 between a microtubule bound and free state. Under disease conditions Tau self-assembles into
49 fibrils that eventually lead to highly insoluble polymeric inclusions known as neurofibrillary
50 tangles. The underlying biophysical basis for the transition of Tau from a microtubule-associated
51 protein to an insoluble fibril is unknown. However, a clue comes from the observation that
52 polyanions, such as heparin, promote Tau fibrillization [1]. Although less effectively, RNA can
53 also induce Tau fibrillization [2, 3], and unlike heparin, RNA is present intracellularly, making it
54 accessible to interact with Tau.

55 Our experiments began with the finding that Tau can bind RNA in living cells and
56 interestingly Tau-RNA binding shows selectivity for tRNAs. This observation along with the
57 known categorization of Tau as intrinsically disordered and its ability to spread from cell to cell
58 in a manner that resembles prions [4, 5], suggested that Tau might share additional properties
59 with other RNA binding proteins involved in neurodegeneration. These proteins include FUS [6],
60 TDP-43 [7], C9ORF72 [8, 9], hnRNPA2B1 and hnRNPA1 [10, 11] all of which can undergo
61 liquid-liquid phase-separation from the surrounding aqueous medium into droplets *in vitro*.
62 These highly protein dense structures, known in the chemical literature as complex coacervates
63 [12, 13], establish a liquid liquid phase state (LLPS) associated with (1) increasing protein
64 concentration, (2) tuning the salt concentration and temperature, (3) the presence of RNA
65 complexed to an intrinsically disordered protein and (4) low interfacial tension to promote fusion.
66 A consensus property of a complex coacervate is high internal fluid dynamics rooted in low

67 cohesive energy between the polyelectrolyte complexes and weakly bound water constituting the
68 fluid [13, 14]. Complex coacervate chemistry has facilitated bio-inspired coating, wet adhesion
69 and engulfment [15-17].

70 Here we show that Tau-RNA complexes have all the properties of a complex coacervate.
71 When multiple Tau molecules weakly bind RNA and overall charge matching is achieved
72 between the polycation, Tau, and polyanion, RNA, Tau undergoes condensation and phase
73 separation into micrometer sized droplets. Remarkably, within this liquid phase-separated state
74 Tau maintains internal segment mobility and a compact conformation between two spin labels
75 around the core region of Tau known as PHF6(*) despite the molecular crowding associated with
76 coacervation. In contrast, this region undergoes irreversible fibrillization in the presence of a
77 different polyanion, heparin, which induces full extension of Tau monomers and packs
78 monomers into β-sheet assemblies. The spontaneous and reversible droplet formation suggests
79 that Tau is held in a low energy-barrier fluid state between dilute solution and complex
80 coacervate condensate with the free energy difference toggled by interactions mediated by ions.
81 However, prolonged residence in this phase state begins to induce β-sheet formation suggesting
82 that the highly condensed phase state of Tau is a precursor to fibril formation.

83

84 Results

85 Tau binds RNA in living cells

86 RNA binding to Tau in living cells was examined by PAR-iCLIP using the human Tau-
87 specific antibody, HJ 8.5, in HEK 293T cells, human iPSC-derived neurons and retinoic acid-
88 differentiated neuroblastoma SH-SY5Y cells. The HEK 293T cells expressed wild type full-
89 length human Tau (4R2N), mutant Tau (P301L-4R2N) or mutant Tau fused to CFP (P301L,

90 4R1N) (Fig. 1a-b, Fig. S1, Fig. S2a-c). iPSC-derived neurons were derived from carriers of
91 4R2N Tau (Fig. 1c), P301L Tau or a risk variant for progressive supranuclear palsy, A152T. The
92 SH-SY5Y cells expressed both Tau and the short isoform of MAP2 called MAP2c [18] (Fig.
93 S2d). Strong binding of Tau to RNA was observed in all cells, as indicated by ^{32}P-labeled RNA
94 bands corresponding to immunoprecipitated and cross-linked Tau-RNA complexes (Fig. 1a-c,
95 lanes 2; Fig. S2a, lane 2). The radioactive Tau-bound RNA band was found to run as 30-100 nt
96 (data not shown). PAR-iCLIP experiments with varying RNase concentrations did not shift the
97 ^{32}P-labeled band, nor change its intensity (lanes 2-3 in Fig. S2b). These experiments indicate that
98 in contrast to most known RNA-binding proteins that bind to RNA as a smear over a range of
99 sizes, Tau binds specifically and dominantly to small RNAs or RNA fragments.
100 Because small RNAs are abundant and may engage in non-specific interactions, we
101 performed multiple confirmatory controls (Fig. S2b lanes 1, 4 and S2c lanes 3, 4), including
102 immunoprecipitation in HEK cells without Tau expression, without Tau antibody to rule out non-
103 specific binding and without UV exposure to eliminate the possibility that Tau-RNA complexes
104 formed *in vitro* after cell lysis. Various disease mutations of Tau had no effect on the binding to
105 RNA in either the HEK cells or the human iPSC-derived neurons. Although Tau and MAP2 are
106 highly homologous in their proline rich and microtubule binding domains, MAP2 did not bind
107 RNA (Fig. S2d, lane 3).
108 To identify the RNA types crosslinked to Tau, DNA libraries were prepared from the
109 immunoprecipitated radiolabeled bands and sequenced. In all experiments, the controls
110 consistently showed relatively few total reads and very few uniquely aligned reads (Fig. S2e-f).
111 We analyzed the distribution of Tau-bound RNA from the human genome by defining eight
112 regions: exons, introns, lincRNAs, snRNAs, rRNAs, miRNAs, tRNAs and intergenics. In Tau-

113 expressing HEK cells, tRNAs were overwhelmingly the highest category of RNA crosslinked to
114 Tau (Fig. 1d). Endogenous Tau in hiPSC-derived neurons also bound tRNAs; however,
115 background RNA from introns and intergenics were relatively abundant as well (Fig. 1e).
116 Background RNA sequences are common in all CLIP studies, particularly for atypical RNA
117 binding proteins [19]. Despite the abundance of tRNAs in cells however, background reads from
118 CLIP experiments consistently show a paucity of tRNAs. Correcting for background reads by
119 dividing the percentage of Tau-bound RNA by the percentage of nucleotides of each category in
120 the genome demonstrated a selective enrichment of tRNAs (Fig. 1f-g). The specific tRNA
121 species crosslinked to Tau overlapped extensively between HEK and hiPSC-derived neuron
122 samples. Of 625 annotated tRNA loci in the human genome, 462 tRNA genes crosslinked to Tau
123 in HEK cells with 79% of them observed in all four Tau CLIP samples and 94% in at least two
124 samples. In the hiPSC-derived neurons, all 231 tRNA genes identified were also observed in the
125 HEK cells and 119 of these were verified in at least two Tau CLIP samples. The distribution of
126 the cross-linked tRNAs in HEK and hiPSC-derived neurons differed from the distribution of the
127 total tRNAs. This difference indicated that the tRNAs selected by the CLIP experiment were not
128 randomly drawn from the total tRNA pool (Fig. S3a-b). Among the most differentially selected
129 tRNAs by CLIP was $tRNA^{Arg}$ (Fig. S3c).
130 PAR-iCLIP can identify the cross-linked sites in the tRNAs. tRNA sequences extend
131 from the most 3' nucleotide of the tRNA to the covalently cross-linked site where the sequencing
132 terminates. In both HEK cells and hiPSC-derived neurons, the crosslink site was predominantly
133 located within the anti-codon loop (Fig. 2a-b, Fig. S4), followed by the T loop and in the D-loop,
134 both with far smaller frequencies. Overall there was a preference for single-strand segments of
135 tRNA as crosslink sites.

136

137 **Tau-RNA Binding Affinity and Stoichiometry**

138 A gel shift assay using recombinant wild type full-length human Tau (4R2N) induced a
139 shift in unacetylated $tRNA^{Lys}$ (Fig. 3a), yielding a dissociation constant (K_d) for 4R2N Tau
140 binding to tRNA of 460 ± 47 nM (Fig. 3b). The derived Hill coefficient was 2.8, implying
141 cooperative binding of multiple Tau proteins to tRNA [20]. Isothermal titration calorimetry (ITC)
142 experiments independently confirmed the affinity of Tau binding to tRNA to yield K_d = 735 ±
143 217 nM and 372 ± 9 nM for 4R2N and K18 Tau, respectively (Fig. 3c). The dissociation constant
144 for 4R2N Tau binding to a 43 nucleotide random RNA sequence still yielded a K_d = 832 ± 94 nM
145 with a Hill coefficient of 2.6 according to a gel shift assay, suggesting that Tau effectively binds
146 RNA non-specifically *in vitro*, although there may be differences in binding affinity.

147 Our *in vitro* observation further suggested that Tau binds RNA in two stages, first
148 forming a protein dimer-RNA (P_2R) complex followed by a protein multimer-RNA ($P_{2n}R$)
149 complex, consistent with a two-stage RNA binding model reported for the protein AUF1 [21]
150 and hnRNP A1 [22]. The ITC titration experiments showed that both 4R2N and K18 Tau interact
151 with tRNA with the stoichiometry of a protein dimer (Fig. 3c, n = 0.52 ± 0.04), while the gel
152 shift assay showed multiple bands corresponding to high molecular weight protein-RNA
153 complexes. These include a faster migrating band representing P_2R complexes populated at
154 lower Tau:tRNA molar ratio and a slower migrating band representing $P_{2n}R$ complexes
155 populated at higher Tau:tRNA molar ratios (Fig. 3d-e). The fraction of bound Tau (from the low
156 or high bands) was plotted as a function of Tau:tRNA molar ratios (Fig. 3f), and compared to the
157 theoretical binding saturation curves for 1:1 to 6:1 binding stoichiometries (Fig. 3f). At lower
158 Tau:tRNA molar ratios, Tau and RNA form complexes at a ~2:1 ratio, while at higher Tau:tRNA

159 molar ratios, Tau and tRNA form complexes at ratios up to 6:1. We conclude that tRNA is
160 capable of binding multiple Tau proteins in a multi-step process. Judging by the absence of
161 higher stoichiometric signatures in the ITC measurement that is less sensitive to binding events
162 associated with small changes in heat, Tau:tRNA complexes that exceed a ratio of 2:1 must rely
163 on weak interactions.
164
165 **Tau phase-separates in the presence of RNA**
166 Mixing of 4R2N or Δtau187 (similar to K18, see Methods section) constructs with tRNA
167 (25 kDa), poly(A) RNA (66~660 kDa) or poly(U) RNA (800~1000 kDa) reliably produced a
168 turbid solution under a wide range of Tau:RNA mass ratios and salt concentrations (Fig. 4a-e and
169 Fig. S5a-e). According to bright-field microscopy (Fig. 4a), droplets formed and phase separated
170 from the bulk aqueous phase with a clearly visible and highly spherical boundary. Tau droplets
171 were capable of merging into a single droplet with the complete and nearly instantaneous loss of
172 any boundary at the fusion interface, indicating that the droplets are fluidic with a relatively low
173 interfacial tension (a series of snapshots capturing the fusion of two droplets are shown in Fig.
174 4a). Confocal microscopy images of fluorescence-labeled Tau verify that Tau is exclusively and
175 homogenously contained within the droplet (Fig. 4b).
176
177 **Tau-RNA droplets form a complex coacervate phase**
178 Droplet formation follows from the mixing of two oppositely charged biopolymers at a given
179 pH—Tau and RNA. Systematic increase in the salt concentration decreased the number of Tau-
180 RNA droplets that eventually disappeared when the salt concentration was increased to 100 mM
181 or higher (Fig. 4c-d, Fig. S5a left panel). Droplet formation was maximal at Δtau187:tRNA

182 molar ratios of 8:1, Δtau187:poly(A) RNA molar ratios from 33:1 to 330:1 and Δtau187:poly(U)
183 RNA ratios from 267:1 to 333:1 (estimated from the molecular weight of RNAs, see Fig. S5c).
184 Remarkably, each of these stoichiometries converge to a Δtau187:tRNA charge ratio of ~1:1,
185 irrespective of the RNA type (Fig. 4e, Fig. S5a right panel). Droplet formation was also
186 observed with full length Tau 4R2N and RNA, but was less robust than with Δtau187, possibly
187 due to the additional negative charges at the N-terminal segment of Tau 4R2N that would
188 diminish the electrostatic association between Tau and RNA. However, at pH 6 where the net
189 charge of Tau 4R2N is similar to Δtau187, droplets reliably formed, though yielding lower
190 number densities, and were exquisitely sensitive to salt concentration (Fig. S5e). Even at NaCl
191 concentrations as low as 10 mM, the droplets dissolved. In cellular environments however,
192 additional factors—charged co-constituents or posttranslational modifications of Tau—may
193 strengthen Tau-RNA associations, rendering droplet formation more favorable at higher ionic
194 strengths. Together, these observations show that droplet formation is dominated by electrostatic
195 complexation between oppositely charged polyelectrolytes, while the shielding of their excess
196 charge (by the tuning of Tau:RNA ratio) is critical to form an extended assembly constituting the
197 droplets. From this we conclude that Tau-RNA droplet formation follows a complex
198 coacervation mechanism, initiated through non-specific complexation of oppositely charged
199 polyelectrolytes and driven by the further association of these polyelectrolyte complexes to form
200 a macroscopic fluid phase by relying on weak electrostatic attractions tuned by salt concentration
201 [23]. A crucial observation is that complex coacervate droplet formation is spontaneous and fully
202 reversible through the tuning of salt concentration and Tau:RNA ratios. The convergence of
203 different Tau constructs toward the shared property of complex coacervation with different RNA

204 species present at a common charge ratio of ~1:1 leads us conclude that complex coacervate-
205 driven droplet formation is an intrinsic property of Tau in the presence of RNA.
206
207 **Tau in condensed droplets is in a solution state**
208 Within a condensed complex coacervate, held together by non-specific and weak electrostatic
209 interactions, we expect the polyelectrolyte constituents to maintain their hydration layer and
210 remain dynamic [14, 24]. To spectroscopically track Tau exclusively from within the condensed
211 phase we first positively verified by confocal fluorescence imaging that Δtau187 was exclusively
212 localized within the droplet (Fig. 4b). This allowed us to characterize the droplet-internal protein
213 properties. First, continuous wave electron paramagnetic resonance (cw EPR) spectral line shape
214 analysis of singly spin labeled Δtau187 at cysteine site 322, Δtau187/322C-SL, diluted with
215 diamagnetically labeled Δtau187/322C-DL (see Methods), was used to compare the protein side
216 chain dynamics and degrees of freedom of the tethered spin label of Δtau187 in dilute solution
217 state (Fig. 4 red, f-h), in the droplet state associated with poly(A) RNA (blue, f) and tRNA (green,
218 g) and upon addition of the Tau aggregation inducer, heparin (black, h). Remarkably, the EPR
219 lineshape of Δtau187/322C-SL within the droplet phase was indistinguishable from the dilute
220 solution state (Fig. 4f vs. 4g). In contrast, the EPR line shape dramatically broadened within
221 minutes of adding heparin—a highly effective aggregation inducer of Tau [1, 25] (Fig. 4f vs. 4h).
222 This finding demonstrates that the condensation of Δtau187 to high protein concentration alone
223 does not effectively induce dehydration and aggregation of Tau, and that Tau remains dynamic
224 and hydrated and retains protein dynamical properties as found in solution state, despite forming
225 long-range associations with RNA in a highly condensed fluid phase.

226 To determine whether Tau assumes altered protein conformations in the complex
227 coacervate phase compared to the dilute solution phase, we compared the PHF6 and PHF6*
228 hexapeptide regions of Tau under these conditions. These regions of the Tau sequence pack into
229 the β-sheet core once fibrils are formed of Tau [26]. Previously, we identified that both the PHF6
230 and PHF6* hexapeptide regions of Tau undergo a dramatic opening from a compact to a fully
231 extended local conformation within minutes of adding heparin, well before fibril formation is
232 seen and remain extended as insoluble fibrils are formed (unpublished data). These local distance
233 measurements of the regions flanking the PHF6(*) regions offer a powerful tool to compare the
234 conformational state of Tau in dilute solution, droplet and aggregation-induced states. We
235 prepared a Δtau187 G272C/S285C-SL_2 construct that was doubly MTSL-labeled at sites 272 and
236 285 (see Methods) to access the distances across the PHF6* hexapeptide region by double
237 electron-electron resonance (DEER) spectroscopy. Surprisingly, the distances flanking the
238 PHF6* region remained unchanged from dilute solution state to when Tau was condensed into a
239 concentrated complex coacervate phase in association with poly(A) RNA and tRNA (Fig. 4i and
240 j). This contrasts with the effect of heparin on Tau that markedly extended the segment distances
241 (from ~3 to ~4 nm) between the labels, within minutes of heparin addition, corresponding to the
242 extended conformation that the PHF6(*) segment adopts in insoluble fibrils when neatly stacked
243 in β-sheets (Fig. 4k).
244 Interestingly, we observed a low-level Thioflavin T (ThT) signal under Tau-poly(U)
245 RNA droplet forming conditions (see Fig. S5f) that gradually increased with time over 12 hours.
246 This ThT signal was nearly entirely diminished at increased salt concentration at which Tau-
247 RNA associations are weakened and droplets are resolved. Still, the ThT intensity from the Tau-
248 RNA droplet samples, even after three days of incubation, was significantly smaller (less than

249 5%) compared to what was observed in the presence of the aggregation-inducing heparin under
250 similar charge ratio and mass concentration at any incubation time (Fig. S5f). Since ThT
251 intensity is commonly used as an assay to map β-sheet content, we suggest that droplet formation
252 through association with RNA increases the aggregation propensity of Tau *in vitro*, even while
253 the Tau-RNA complexes are held together by fully reversible weak interactions.
254
255 **Exogenous tRNA can induce sarkosyl insolubility of Tau**
256 To determine whether Tau-RNA complexes have the potential for pathological
257 interactions *in vivo*, hiPSC-derived neurons with a P301L mutation or wild type were transfected
258 with 20U tRNA per 1.2 million cells. Cell lysates (input) were prepared in a high salt/high
259 sucrose buffer, followed by fractionation in a 1% sarkosyl buffer. Transfection in the absence of
260 nucleic acids (mock) or addition of tRNA to the mock lysate (mock + tRNA) were used as
261 controls. Cells transfected with tRNA accumulated sarkosyl insoluble Tau, whereas cells without
262 added tRNA or when tRNA was added to the lysis buffer did not increase Tau in the insoluble
263 fractions (Fig. 5). The increase in sarkosyl-insoluble Tau populations occurred in both wild-type
264 and P301L Tau-containing cells when infected with tRNA.
265
266 ## Discussion
267 Tau can bind RNA in two stages, mediated by (i) strong binding at a Tau:RNA molar
268 ratio of 2:1 with nanomolar dissociation constants and (ii) weak association between Tau
269 multimers and RNA to form higher order complexes. Although Tau lacks a recognizable RNA-
270 binding motif, it bound tRNA as its dominant partner *in vivo*. Furthermore, Tau was found to
271 spontaneously phase separate upon non-specific complexation with RNA into dense protein

272 droplets, whose formation was reversibly and sensitively tunable by salt concentrations, as well
273 as the Tau:RNA ratios. Crucially, the optimal Tau:RNA molar ratios range from 8:1 to 330:1,
274 which varies among different RNA species. Remarkably, all higher order complexes converge to
275 a common Tau:RNA charge ratio of ~1:1, leading us to conclude that Tau-RNA droplet
276 formation is driven by electrostatic interactions underlying complex coacervation, in which
277 oppositely charged polyelectrolytes associate into extended assemblies held together by weak
278 electrostatic interactions and condense to a macroscopic fluid phase [14, 17, 27].

279 Crucially, Tau complexed with RNA in the highly condensed droplet state maintains the
280 dynamical and conformational signature of free Tau in solution state according to cw EPR and
281 DEER analysis around the β-sheet forming PHF6(*) segment of Tau, implying that small
282 changes in the free energy of Tau accompany its condensation to the droplet phase. At the same
283 time, a low-level ThT signal was observed from the Tau-RNA droplet samples after extensive
284 incubation time, though significantly weaker compared to from Tau solutions *en route* to fibrils
285 as initiated by the addition of heparin. Nevertheless, the implication that Tau droplets have some
286 propensity toward soluble β-sheet complexes suggests that complexation with RNA under
287 droplet forming conditions may be on pathway to fibrils. Consistent with this finding, tRNA
288 increased sarkosyl insolubility of Tau *in vivo*. We conclude that dynamic and free Tau species
289 are stored in the concentrated droplet state that, on the one hand is predisposed to convert to
290 fibrils, and on the other hand can spontaneously and reversibly dissolve into solution at increased
291 salt concentration. This previously unrecognized droplet phase state contrasts with that of Tau
292 following incubation with the polyanion, heparin, in which an irreversible transformation to
293 fibrils occurs and a large intra-Tau conformational change is observed in solution state preceding
294 fibril formation.

295 RNA generally promotes complex coacervation whereas heparin effectively promotes
296 fibrillization of Tau. The distinguishing effects between RNA (a polyphosphate) and heparin (a
297 polysulfate) on Tau—coacervation versus fibrillization—may be an operational principle of Tau-
298 polyanion association. Weak associations between multiples of Tau and RNA is consistent with
299 the consensus property of a coacervate phase in which the hydration layer of the polyelectrolyte
300 constituents remains intact, ensuring fluidity of the condensed phase, as well as reversibility
301 between the dilute and condensed phase [14]. The Tau droplet state fits this biochemical portrait,
302 so that Tau can reversibly and rapidly switch between the dilute solution and the dense droplet
303 state, while involving minimal rearrangement of hydration water and protein conformations. The
304 spontaneous complex coacervation from synthetic polyelectrolyte constituents can be entropy-
305 driven according to several studies [6, 23, 28-30]. We found that Tau-RNA complex
306 coacervation was enhanced at elevated temperatures, consistent with an entropy-driven reaction
307 (data not shown). In fact, the observation of solution state-like protein conformational dynamics
308 of Tau in the coacervate phase implies that the free energy penalty due to lowering of protein
309 configurational entropy from protein ordering is minimal in the droplet state, and thus the cost
310 for an entropy-driven complex coacervation reaction, paid by salt and/or water release, is small.
311 Given this insight, we conclude that the transformation to insoluble aggregates from Tau droplets
312 should be energetically more favorable than from dilute solution state, given the elevated protein
313 concentration in the complex coacervate phase. Along these lines ten Wolde and Frenkel [31]
314 have proposed that condensed liquid droplets serve as a "metastable crucible" to lower free
315 energy barriers for crystal nucleation, while the discovery of the involvement of nucleic acids in
316 coacervation-driven phase separation dates back to 1949 by Bungenberg de Jong [15]. Here, we
317 identify a new state of Tau in which soluble Tau is reversibly stored in concentrated complex

318 coacervate droplets, readily bioavailable for cellular functions or vulnerable to pathological
319 aggregation depending on the environmental cues at hand.
320

321 Materials and Methods

322 **Cell culture**

323 A total of eight samples were used for PAR-iCLIP studies. Four samples were human embryonic
324 kidney (HEK 293T) cells that expressed either 4R2N (residues 1-441) wild type *tau* (one
325 sample), 4R2N *tau* harboring the P301L mutation (one sample), and 4R1N *tau* harboring the
326 P301L mutation fused to CFP (2 samples). Four samples were neurons derived from human
327 induced pluripotent stem cells (hiPSCs) obtained by reprogramming dermal fibroblasts with
328 virally transduced Yamanaka factors [32] that expressed wild type *tau*, two harboring a P301L
329 *tau* mutation (with and without fused CFP) and one harboring the A152T variant [33, 34]. The
330 hiPSC lines were karyotyped by Cell Line Genetics. Both wild type and P301L were normal
331 males (46XY). A152T displayed a balanced three-way translocation of chromosomes 1, 13 and 7,
332 which most likely occurred during the reprogramming process (46XY, t(1;13;7)
333 (q31.2;q21;q36.3). Pluripotent cells were maintained in feeder-free conditions and cultured in
334 BD Matrigel (BD Biosciences) coated six-well plates and fed with mTSER daily (Stemcell
335 Technologies). Neuroectoderm differentiation utilized dorsomorphin and SB431542 (Sigma-
336 Aldrich) for a week [35]. When neural-rosettes were clearly observable, the media was gradually
337 replaced with neuronal induction media containing Knockout DMEM F12 with N2, and
338 Glutamax 1X supplemented with laminin (Sigma-Aldrich) and maintained for an additional six
339 days with every other day feeding. Neuro-rosettes were microdissected, and grown as
340 neurospheres in the neuronal induction media supplemented with B27. Neurons were

341 differentiated from neurospheres by dissociating them into individual cells enzymatically with a
342 1/1 mixture of 0.25% trypsin / StemPro accutase (Thermo Fisher), and plated on Poly-L-
343 Ornithin/Laminin coated six well plates at a density of 200,000 cells per well. Neuron
344 differentiation and maturation were stimulated by the addition of 10 mM each of NT3, BDNF,
345 and GDNF (Preprotech) to the neuronal growth media containing Neurobasal, N2 supplement,
346 B27 Supplement and Glutamax. Neurons were fed twice per week by replacing half of the
347 conditioned media with pre-warmed supplemented fresh media, and underwent maturation for at
348 least five weeks. SH-SY5Y Neuroblastoma cells were plated as monolayers in DMEM/F12
349 medium with 10% FBS at 1x 10^6 per 10 cm dish, and the cells switched to neurobasal medium
350 the next day and differentiated for seven days using 10 μM retinoic acid.
351
352 **Antibodies**
353 The Tau antibodies used were Tau-5 (1 mg/ml, Abcam); HJ 8.5 and HJ 9.2 (4.5 mg/ml and 2.8
354 mg/ml, both HJ antibodies are gifts from Dave Holtzman, Washington University); PHF-1 (gift
355 from Peter Davis, Albert Einstein College of Medicine), MAP2 antibody (0.3 mg/ml,
356 Proteintech™); CDK5 rabbit antibody (0.2 mg/ml, Santa Cruz); GFP rabbit antibody (5 mg/ml,
357 Abcam); β-Actin (Sigma-Aldrich); mouse IgG_1 Alexa 680, (2 mg/ml, Invitrogen); mouse IgG
358 Alexa 680 (2 mg/ml, Invitrogen); rabbit IgG 800 (1 mg/ml, Odyssey).
359
360 **PAR-iCLIP**
361 Cells were treated with 4-thiouridine (4SU) (Sigma-Aldrich) for 1h at a final concentration of
362 500 μM at 37°C, rinsed with ice-cold 1x PBS and irradiated one time with 400 mJ/cm^2 of
363 365 nm UV light on ice. 4-SU can enhance the cross-linking efficiency especially for proteins in

364 the cytoplasm [36-38]. The cells were centrifuged and the pellet stored at -80°C. The major steps
365 of PAR-iCLIP are listed in Fig. S6 and detailed in the supporting information. CLIP experiments
366 require an antibody, which can effectively immunoprecipitate Tau under stringent high salt wash
367 conditions. HJ 8.5 [39] raised against human Tau efficiently depleted Tau. With a dissociation
368 constant of 0.3 pM, HJ 8.5 pulled down Tau under the high-stringency purification conditions of
369 CLIP and remained bound to Tau throughout the procedure. Control experiments with GFP or
370 CDK5 antibody for the lysate expressing those proteins, or with HJ 8.5 antibody for lysates
371 without expressing Tau were always done in parallel to rule out false positive binding caused by
372 the beads. After immunoprecipitation, the cross-linked RNA was radiolabeled, the protein
373 separated on an SDS-PAGE gel, and transferred to nitrocellulose membrane and blotted. The
374 RNA-protein complexes from CLIP experiments (Fig. 1a-c) were cut from the blot, and the RNA
375 extracted followed by reverse transcription for library preparation [36]. The ^{32}P-labeled RNA
376 band was run on a polyacrylamide Tris-Borate Urea (TBU) denaturing gel to demonstrate the
377 confirm the size of the complex.
378
379 **Library preparation, deep sequencing and bioinformatics analysis of iCLIP**
380 The iCLIP libraries contained an experimental and a random barcode, which allowed
381 multiplexing and the removal of PCR duplicates. After the barcodes were introduced, sample and
382 control from one set of experiments were mixed to remove batch-to-batch variation. Libraries
383 were sequenced on an Ion Torrent Proton. Fastx collapser from FASTX-Toolkit was used to
384 collapse reads and filter replicates resulting from the PCR based on the random barcode. Reads
385 were separated into samples by the barcodes at the 5` ends of reads. The reverse transcription
386 primers sequences at both ends of the reads were trimmed with Cutadapt [40]. After trimming

387 the barcodes, reads with 18 bps or more were kept and counted as total unique reads, and aligned
388 to the human genome (hg19) by Bowtie2 [41]. RseQC [42] was used to evaluate the quality of
389 sequencing and mapping reads. Alignments with scores equal or greater than ten were kept for
390 downstream analysis. Reads from these RNA pools were clustered by their alignments, and
391 Pyicos tools [43] were used to identify the significant clusters. Clusters with at least five reads
392 were retained and considered to contain target sites for RNA-Tau crosslinking. Gene models for
393 RefSeq mRNAs, tRNAs, rRNAs were downloaded from the UCSC genome browser. miRNAs
394 were downloaded from miRBase (release 20) and other categories of RNAs were download from
395 Ensemble (release 73). Cross-link sites were identified as the termination site of the sequencing
396 based on the iCLIP protocol [44]. Individual tRNA genes from the UCSC genome browser were
397 predicted by using tRNAscan-SE v.1.23. The secondary structure for each tRNA was obtained
398 from GtRNAdb (http://gtrnadb.ucsc.edu/).
399
400 **Deep sequencing and analyses of small RNA expression in HEK cells and hiPSC-derived**
401 **neurons**
402 Small RNAs were extracted from HEK cells and hiPSC-derived neurons using miRNA isolation
403 kit (mirVana™. Library preparation was adapted from the Ion RNA-seq v2 (Thermo Fisher)
404 protocol. cDNAs with size range from 30-100 bp were selected and sequenced. Reads were
405 aligned to both human genomes and tRNA sequences. When mapping reads to tRNA sequences,
406 the Bowtie read aligner [45] protocol was used, in which a maximum of two mismatches were
407 allowed. Reads aligned to tRNAs were counted and analyzed with a custom Perl scripts.
408
409 **Recombinant Tau and Tau fragments**

410 Full length recombinant human 4R2N Tau, N-terminal truncated, microtubule binding domain
411 containing, K18 Tau (residues 244-372) and Δtau187 (residues 255-441 with a His-tag at the N-
412 terminus) were used for *in vitro* studies. Methods for expression and purification of all
413 recombinant Tau variants are detailed in the supplementary text. Two variants of Δtau187 were
414 prepared via site-direct mutagenesis: Δtau187/322C contains a C291S mutation, leaving only one
415 cysteine at site 322, and Δtau187G272C/S285C contains C291S, C322S, G272C and S285C
416 mutations, leaving two cysteines at sites 272 and 285).
417
418 **RNA gel mobility shift assay**
419 The gel shift assay was performed with recombinant full length 4R2N Tau and
420 chromatographically purified unacetylated yeast $tRNA^{Lys}$ (tRNA Probes) in 100 mM sodium
421 acetate buffer at pH 7.0. The molar concentration of $tRNA^{Lys}$ was accurately re-measured with
422 UV spectrophotometry after base-hydrolization to account for the hyperchromic effect from the
423 secondary and tertiary structure of tRNA [20]. RNA43 was purchased in a kit (Pierce) with the
424 sequence 5'-CCUGGUUUUUAAGGAGUGUCGCCAGAGUGCCGCGAAUGAAAAA-3' to
425 represent a random sequence. The hydrolyzed tRNA and RNA43 samples were then quantified
426 with UV spectrophotometry at 260 nm using an extinction coefficient of 0.025 $(\mu g/ml)^{-1}cm^{-1}$. For
427 the gel shift assay, protein was incubated with tRNA at 37℃ for 10 minutes in the presence of
428 0.5 mM EDTA, 0.5 mM $MgCl_2$, 2 U SUPERase• In™ RNase Inhibitor (Thermo Fisher), 0.01%
429 IGEPAL CA-630 (Sigma-Aldrich), and then applied to a TBE 8% Polyacrylamide Gel (Thermo
430 Fisher). After gel separation, tRNA was stained with SYBR Gold II (Thermo Fisher). For
431 quantitative analysis, the fraction of free and bound tRNA was quantified in ImageJ2 (National
432 Institute of Health).

433

434 **Isothermal Titration Calorimetry (ITC) experiments**

435 Full length Tau or the K18 Tau were dialyzed overnight into a specified buffer for ITC (20 mM
436 ammonium acetate, pH 7). tRNA (from Baker's yeast, Sigma-Aldrich) was re-suspended in the
437 ITC buffer and concentration determined using a Nanodrop 1000 (Thermo Scientific).
438 Experiments were run on a Nano ITC (TA Instruments), in which 300 μM tRNA was titrated (5
439 μl injections) into a 1 ml protein solution of 30 μM Tau. Data was analyzed using the
440 NanoAnalyze v3.6 software (TA Instruments). After substracting the heat generated by tRNA
441 titration into empty buffer, the experimental data was fitted with an Independent binding model.
442 Experiments were repeated in triplicates and standard error of the mean reported.

443

444 **Spin labeling of Δtau187**

445 To achieve labeling with paramagnetic or diamagnetic probes, the protein was dissolved in 6 M
446 guanidinium hydrochloride and labeled overnight at 4°C using a 20-fold molar excess of the spin
447 label (1-oxyl-2,2,5,5-tetramethylpyrroline-3-methyl) methanethiosulfonate (MTSL, Toronto
448 Research Chemicals) or the diamagnetic analog of MTSL (1-Acetoxy-2,2,5,5-tetramethyl-δ-3-
449 pyrroline-3-methyl) methanethiosulfonate (Toronto Research Chemicals). Excess label was
450 removed using a PD-10 desalting column (GE Healthcare) equilibrated in a 20 mM ammonium
451 acetate buffer at pH 7.0. The protein was concentrated using a 3 kDa centrifugal filter (Amicon
452 UFC800396). The final protein concentration was determined by UV-Vis absorption at 274 nm
453 using an extinction coefficient of 2.8 $cm^{-1}mM^{-1}$, calculated from extinction coefficient of
454 Tyrosine [46]. The two variants Δtau187/322C and Δtau187G272C/S285C were spin labeled
455 with paramagnetic MTSL probes at the one or two cysteine sites, and are respectively referred to

456 as Δtau187/322C-SL and Δtau187G272C/S285C-SL_2. In order to achieve spin dilution,
457 Δtau187/322C and Δtau187G272C/S285C were also labeled with the diamagnetic analogue of
458 MTSL probes, and are referred to as Δtau187/322C/322C-DL and Δtau187G272C/S285C-DL_2.
459 Images in Fig. 4a-b were taken using 400 μM Tau, 800 μg/ml poly(A) RNA and 30% glycerol in
460 20 mM ammonium acetate at pH 7.
461
462 **Preparation of Tau-RNA complex coacervate**
463 Droplets were formed in the 20 mM ammonium acetate buffer with NaCl concentration varying
464 between 0 and 100 mM and glycerol concentration from 0 to 50% v/v. Solutions of Δtau187 or
465 full length 4R2N Tau was mixed with tRNA (Baker's yeast, Sigma-Aldrich), poly(A) RNA or
466 poly(U) RNA (Sigma-Aldrich) at varying protein, RNA, NaCl and glycerol concentrations in a
467 0.6 ml Eppendorf tube. RNAs were weighted out as powder and the mass concentration was
468 calculated. The Tau:RNA mass ratio, the total concentration of Tau and RNA, as well as the
469 NaCl salt concentration were optimized to maximize droplet formation, while choosing a total
470 biopolymer density to avoid overlapping of droplets in the images to simplify the calculation of
471 droplet coverage. Microscopy images were acquired at 10 minutes after mixing. A concentration
472 of 19% v/v for the viscogen glycerol was determined to be an optimal concentration to ensure
473 cryoprotection for DEER measurements carried out at ~80 K, while also ensuring maximal
474 droplet formation at room temperature (Fig. S5b).
475 The charge of a peptide at a given pH was estimated by applying an algorithm adapted from
476 Innovagen's Peptide Property Calculator (http://pepcalc.com/). All residues were assumed to
477 have pKa values that are equivalent to the isolated residues (CRC Handbook of Chemistry and
478 Physics, 87th ed). Charges of the C-terminus or N-terminus were estimated as -1 and +1,

479 respectively at both pH 6.0 and pH 7.0. The processing code is made available as supplementary
480 files on the free web (https://github.com/yanxianUCSB/PeptideChargeCalculator).
481
482 **Bright-field microscopy of Tau-RNA droplets**
483 Immediately after mixing Tau in a 0.6 ml Eppendorf tube with RNA under droplet forming
484 conditions (established above) and ensuring thorough mixing, 1 μl of this mixture was applied to
485 a microscope slide that is closed with a cover slide gapped by two layers of double-side sticky
486 tape to generate a liquid sample region with consistent thickness. The microscope slide was kept
487 at room temperature for 10 minutes with the cover slide facing down, during which the particles
488 within the liquid sample region settled down onto the surface of the cover slide. Images were
489 taken with a 12-bit CCD camera across the entire sample liquid region near the surface of the
490 cover slide using an inverted compound microscope (Olympus IX70). Before imaging, Köhler
491 illumination was applied and the focus close to the surface of the cover slide optimized to
492 enhance the contrast between the dark droplets and the bright background.
493
494 **Confocal microscopy of Tau-RNA droplets**
495 For confocal microscopy, Δtau187/322C was fluorescently labeled (Δtau187/322C-FL) with
496 Alexa Fluor 488 C_5 Maleimide (Thermo Fisher) at the same 322 site as Δtau187/322C-SL. 50
497 μM of Δtau187/322C-FL was mixed with 350 μM Δtau187/322C-SL at a 1:7 molar ratio in order
498 to prevent saturation. 800 μg/ml of poly(A) RNA was further added to this Tau solution,
499 resulting in droplet formation in the 20 mM ammonium acetate buffer and in the presence of 20
500 mM NaCl. 10 μL of the mixture was pipetted and put on a microscope slide with a cover slide

501 gapped by double-sided sticky tape. Confocal images were acquired using a spectral confocal
502 microscope (Olympus Fluoview 1000).
503
504 **Droplet quantification from image analysis**
505 To quantify the amount of droplet formed under the given experimental condition of interest,
506 images were taken by a 12-bit CCD camera of an inverted compound microscope (Olympus
507 IX70), and recorded in TIF format. With illumination and focus optimized, droplets settling on
508 the cover slide have lower intensity than their surrounding on the images. An image of the 20
509 mM ammonium acetate buffer was taken to calculate the average intensity to set as threshold in
510 order to classify different parts of the image into droplets and buffer. For each image, the area of
511 the droplets was divided by the total area of the image, generating a % droplet coverage value on
512 the cover slide. Droplets with eccentricity above 0.9 or equivalent diameter below 1 μm were
513 filtered out in order to reduce false reading. The MATLAB code is made available as
514 supplementary files on the free web (https://github.com/yanxianUCSB/DropletAnalysis).
515
516 **Continuous wave (cw) Electron Paramagnetic Resonance (EPR)**
517 Cw EPR relies on the anisotropy of nitroxide radical's Larmor frequency and hyperfine coupling
518 that makes its lineshape highly sensitive to the local dynamics, orientation and confinement of a
519 nitroxide-based spin label tethered to the protein. Cw EPR measurements were carried out with
520 Δtau187/322C-SL using a X-band spectrometer operating at 9.8 GHz (EMX, Bruker Biospin)
521 and a dielectric cavity (ER 4123D, Bruker Biospin). Samples were prepared by either mixing
522 200 μM Δtau187/322C-SL with 300 μM unlabeled Δtau187/322C (to generate 40% spin labeled
523 sample) or by using 500 μM Δtau187/322C-SL (100% labeled). Viscogen was added to the

524 sample to achieve either 19% v/v glycerol (for the droplet samples) or 30% v/v sucrose (for the
525 aggregated samples) matching the DEER conditions. Tau samples under droplet forming
526 condition were prepared by adding 1.5 mg/ml RNA, and Tau samples under aggregation-
527 inducing conditions prepared by adding 125 μM heparin (11 kDa average MW, Sigma-Aldrich).
528 A sample of 3.5 μL volume was loaded into a quartz capillary (VitroCom, CV6084) and sealed
529 at one end with critoseal and the other with beeswax, and then placed in the dielectric cavity for
530 measurements. Cw EPR spectra were acquired using 2 mW of microwave power, 0.3 gauss
531 modulation amplitude, 150 gauss sweep width and 25 scans for signal averaging.
532
533 **Double Electron Electron Resonance (DEER)**
534 DEER measurements were performed on a Q-band pulsed EPR spectrometer operating at 32
535 GHz (E580, Bruker Biospin) equipped with a QT2 resonator (measurements done by courtesy of
536 Bruker Biospin). Samples were prepared by mixing 50 μM Δtau187G272C/S285C-SL_2 with 500
537 μM analog-labeled Δtau187G272C/S285C-DL_2 at a 1:10 molar ratio to achieve spin-dilution and
538 avoid artifacts from unwanted inter-protein spin distances. For DEER, Tau samples under droplet
539 forming condition were prepared by adding 1.65 mg/ml RNA and ensuring 19% v/v glycerol
540 concentration, and Tau samples under aggregation-inducing conditions prepared by adding 137.5
541 μM heparin and ensuring 30% v/v sucrose concentration. 40 μL samples containing 550 μM
542 concentration of Tau were loaded into a quartz capillary (2.4 mm od x 2 mm id) and flash frozen
543 in liquid nitrogen after 20 minutes of incubation at room temperature. DEER measurements were
544 conducted using the dead-time free four-pulse DEER sequence at 80 K, using 22 ns (π/2) and 44
545 ns (π) observe pulses and a 30 ns (π) pump pulse. The raw DEER data was processed using
546 Gaussian fitting via DeerAnalysis2013 [47].

547

548 **Quantification of fibril using Thioflavin T assay**

549 18 μM Δtau187 was mixed with 100 μg/ml poly(U) RNA and incubated at room temperature at
550 presence of 4 μM Thioflavin T for over 3 days with or without additional 100 mM NaCl.
551 Fluorescence at 485 nm was measured via Infinite 200 Pro plate reader (Tecan).

552

553 **Transfer RNA transfection**

554 Neuronal cultures were transfected with 20U of bovine liver tRNA (Sigma-Aldrich) per six well
555 plate using lipofectamine 2000 transfection reagent (Thermo Fisher) following the
556 manufacturer's protocol. Control cells were transfected in equal conditions in the absence of
557 nucleic acid (Mock transfection). Mock transfected cells were lysed as described below, with or
558 without 20U tRNA added to the lysis buffer.

559

560 **Sarkosyl insolube Tau isolation and western blotting**

561 Separation of sarkosyl insoluble Tau was done as described in the literature [48, 49]. Briefly,
562 adherent neuronal cell cultures were lysed with an ice-cold high salt/high sucrose Tris HCl buffer
563 (0.8 M NaCl, 10% Sucrose, 10 mM Tris HCl pH 7.4) containing a 1X Protease Inhibitor Cocktail,
564 and a 1X Phosphatase Inhibitor Cocktail. Lysis proceeded at 4°C for 30 min before detachment
565 with a cell scraper, followed by mechanical dissociation using a micropipette. Immediately
566 afterwards, the lysates were centrifuged at 4°C 3000 x g for 15 min in a microcentrifuge. The
567 clear supernatants were collected and sampled (Input). Sodium lauroyl sarcosinate (Sigma-
568 Aldrich) was then added to the supernatants to a final concentration of 1%, followed by a brief
569 vortexing. Samples were incubated at 4°C with continuous rocking. Samples were then

570 centrifuged at 4°C for 2 h at 170000 x g in a Beckman Coulter 70.1 Ti rotor. Sarkosyl soluble
571 supernatants (Sol.) were collected. Sarkosyl insoluble (Ins.) pellets were resuspended in 2X
572 sample loading buffer (250 mM Tris HCl pH 6.8, 10% Glycerol, 10% SDS, 0.5% bromophenol
573 blue, 20 mM DTT) and heated to 95°C for 10 min. The previously collected input and the
574 sarkosyl soluble fractions were diluted with the same sample loading buffer, and heated under
575 similar conditions. Proteins were separated on a 10% SDS-PAGE, transferred to Nitrocellulose
576 membranes, and blotted with either PHF-1 or β–actin antibody.
577
578 **Data availability**
579 The data that support the findings of this study are available from the corresponding authors on
580 request.
581

582 ## Acknowledgments

583 We are grateful to the Tau consortium for financial support to K.S.K. and S.H., D. M. Holtzman,
584 Washington University School of Medicine for the generous gift of HJ 8.5 antibody and P.
585 Davies, Albert Einstein College of Medicine for PHF-1 antibody. This work was supported by
586 the 2011 NIH Director New Innovator Award to S.H and made use of the Material Research
587 Laboratory (MRL) Central Facilities supported by the National Science Foundation (NSF)
588 through the Materials Research Science and Engineering Center under Grant DMR 1121053. We
589 acknowledge the use of the NRI-MCDB Microscopy Facility and the Spectral Laser Scanning
590 Confocal supported by the Office the Director, National Institutes of Health (NIH) under Award
591 # S10OD010610. The authors declare no competing financial interests.
592

593

Figure 1

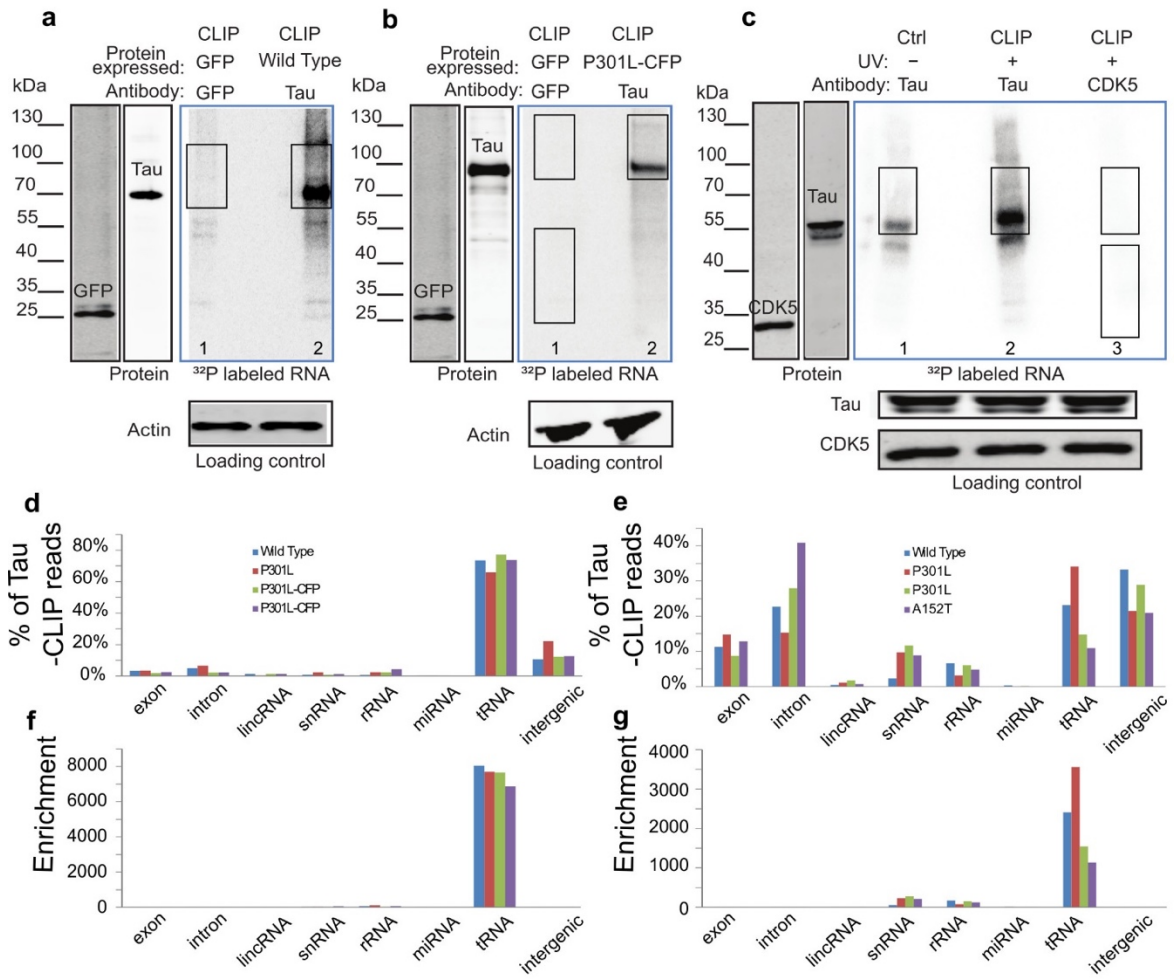

594

595 **Fig. 1: Tau PAR-iCLIP in Tau expressing HEK cells and hiPSC-derived neurons.** Phosphor

596 images in the blue frame display crosslinked ^{32}P-labelled RNA in the nitrocellulose blot. (a-c)

597 PAR-iCLIP with wild type Tau (a) or Tau P301L-CFP (b) and endogenous wild type Tau in

598 hiPSC-derived neurons (c) (lane 2 in a-c), PAR-iCLIP for GFP (lane 1 in a-b), CDK5 (lane 3 in c)

599 and no UV control (lane 1 in c). The antibodies anti-Tau HJ 8.5, anti-GFP and anti-CDK5 were

600 used for protein precipitation. No RNase was added. A small RNA signal was visible in the

601 absence of cross-linking in hiPSC-derived neurons (lane 1, c), suggesting a small portion of

602 RNA may associate with Tau *in vitro* after cell lysis. The RNA-protein complexes from CLIP
603 marked by a rectangle was cut from the blot for DNA library preparation. (d-e) % of Tau-CLIP
604 reads that mapped to eight human genome regions in HEK cells (d) and hiPSC-derived neurons
605 (e). (f-g) Enrichment of tRNA in Tau-CLIP of HEK cells (f) and hiPSC-derived neurons (g) as
606 discussed in text.
607

607

Figure 2

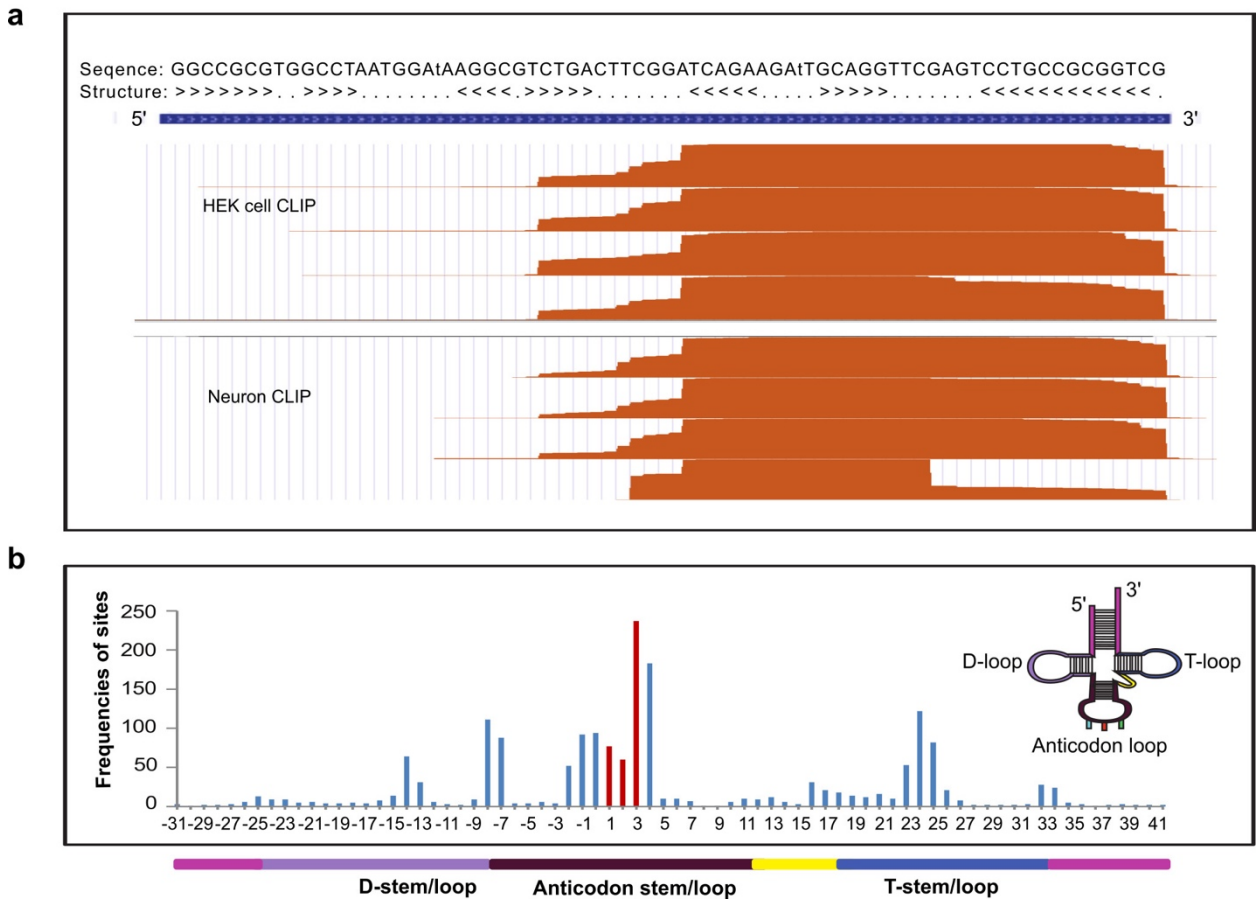

608

609

610 **Fig. 2: Enrichment of tRNA in PAR-iCLIP data.** (a) CLIP cDNA reads for tRNA

611 chr15.tRNA4-ArgTCG are found in all CLIP samples and demonstrate a similar pattern of

612 crosslinking. (b) Analysis of crosslinked sites along tRNA secondary structure demonstrates the

613 anticodon preference, anticodon (colored red) designated as position 1-3 for alignment purpose.

614 The colored illustration of tRNA secondary structure is displayed as inset and below the x-axis in

615 1-D dimension.

616

616
617

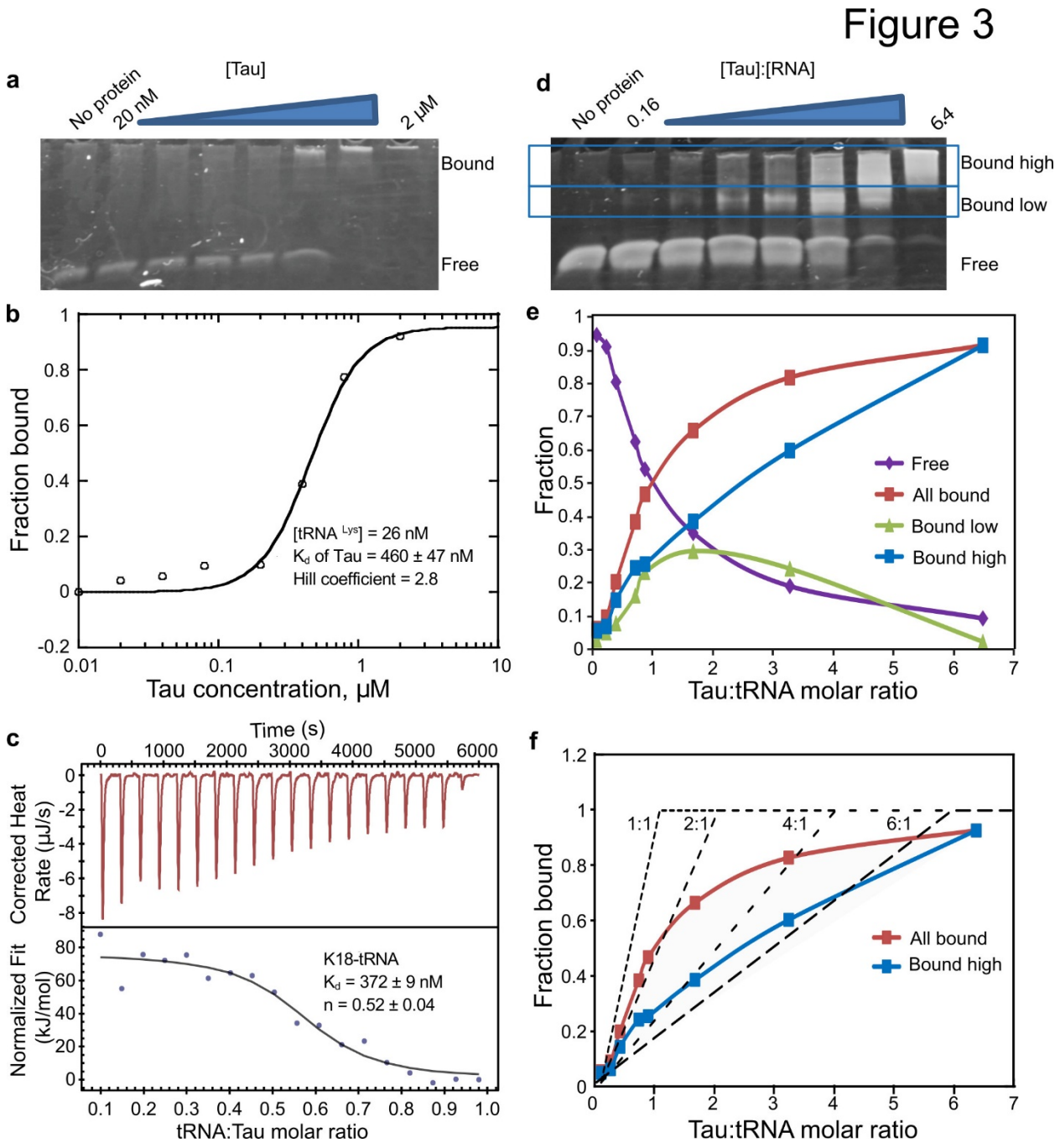

618

619

620 **Fig. 3: Tau tRNA binding by gel shift assay and ITC.** (a) Direct titration experiment shows

621 full length protein Tau induces a mobility shift in $tRNA^{Lys}$. (b) The fraction of bound tRNA

622 plotted as a function of the monomeric Tau concentration and fit to the Hill equation, y = 1/ [1+

623 $(K_d / x)^n$. (c) Yeast tRNA was titrated into solutions of K18 Tau in an ITC experiment. The top
624 panels show the raw incremental-titration. The area under each peak is integrated and plotted
625 against the molar tRNA:Tau ratio and fitted to an independent binding model (the bottom panel).
626 (b-c) Standard error of the mean (SEM) is reported, n=3. (d) Stoichiometry shift assay varying
627 full length protein Tau:RNA molar ratio while tRNA in 2.6 μM. (e) Fraction of bound tRNA in d
628 is plotted over the molar Tau:tRNA ratio. (f) Fraction of bound Tau plotted as a function of
629 Tau:tRNA molar ratios and compared to the theoretical saturation binding curves (dotted
630 lines) with 1:1 to 6:1 protein:RNA molar stoichiometry.

Figure 4

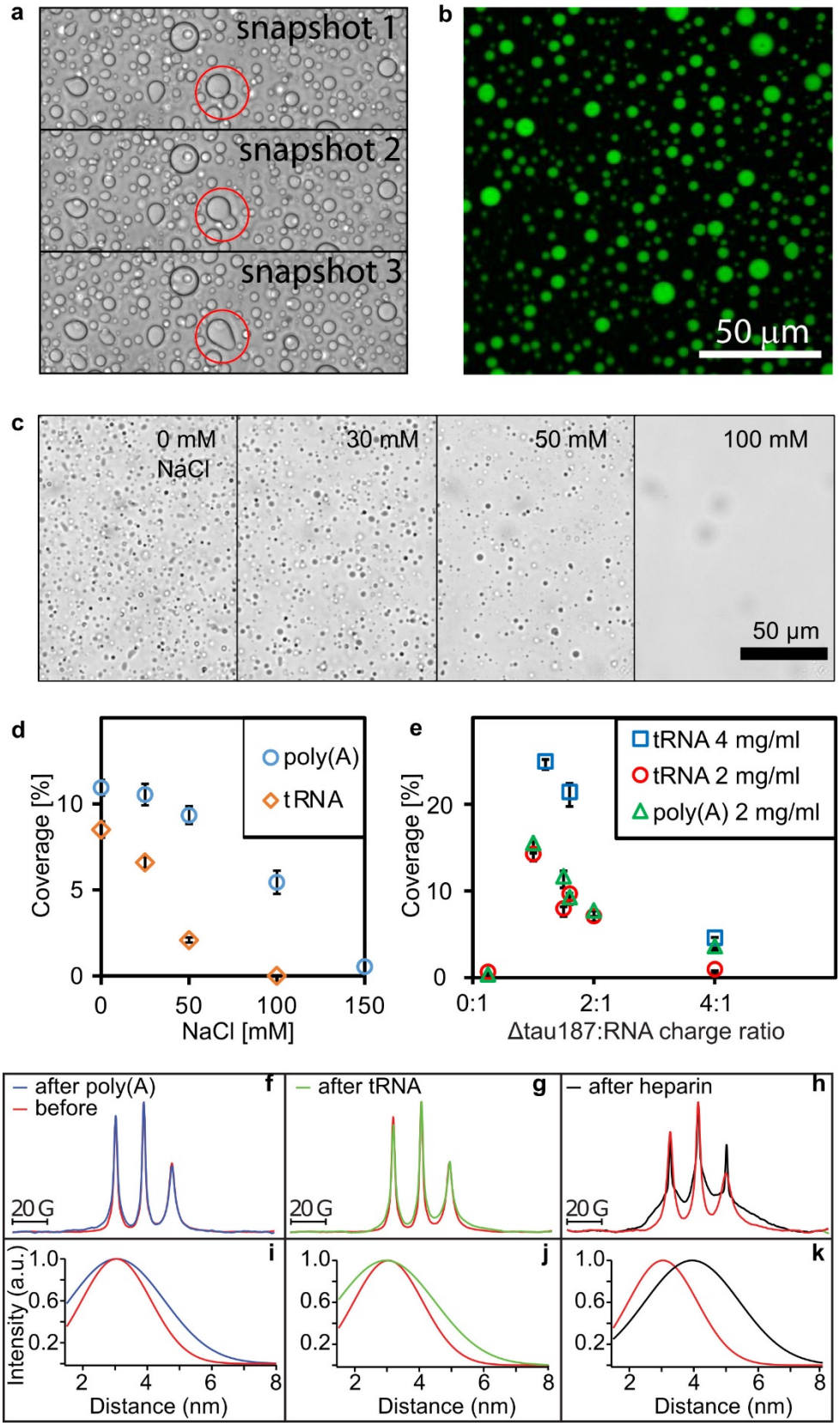
a
snapshot 1
snapshot 2
snapshot 3
b
50 µm
c
0 mM NaCl
30 mM
50 mM
100 mM
50 µm
d
poly(A)
tRNA
Coverage [%]
NaCl [mM]
e
tRNA 4 mg/ml
tRNA 2 mg/ml
poly(A) 2 mg/ml
Coverage [%]
0:1
2:1
4:1
Δtau187:RNA charge ratio
after poly(A)
before
f
after tRNA
g
after heparin
h
20 G
i
j
k
Intensity (a.u.)
Distance (nm)

631

632 **Fig. 4: Tau and RNA forms droplet *in vitro*.** (a) Bright field snapshots of droplets from
633 Δtau187 and poly(A) showing two droplets seamlessly fusing (highlighted with red circle). (b)
634 Confocal microscopy image of Δtau187 labeled with Alexa-488 in the droplets as in (a). c)
635 Representative bright-field images of Tau-RNA droplet with varying [NaCl]. d) Droplet
636 coverage with poly(A) or tRNA with varying [NaCl] and e) varying Δtau187: RNA charge ratios.
637 Δtau187:RNA in c-d were maintained at a charge ratio of 1.2:1 and a total mass concentration of
638 2 mg/ml. Error bars in (d) and (e) represent the standard deviation from n=3. (f-k) CW EPR
639 spectra obtained at room temperature of Δtau187 in droplets formed with 1.5 mg/ml poly(A)
640 RNA (f) and 1.5 mg/ml tRNA (g) is unaltered from solution before adding RNA. CW EPR line
641 shape upon adding 125 μM heparin (h) show dramatic line broadening. DEER of Δtau187-SL_2 in
642 droplets formed with 1.5 mg/ml poly(A) RNA (i) and 1.5 mg/ml tRNA (j), as well as upon
643 incubation with 137.5 μM heparin (k).
644

644

Figure 5

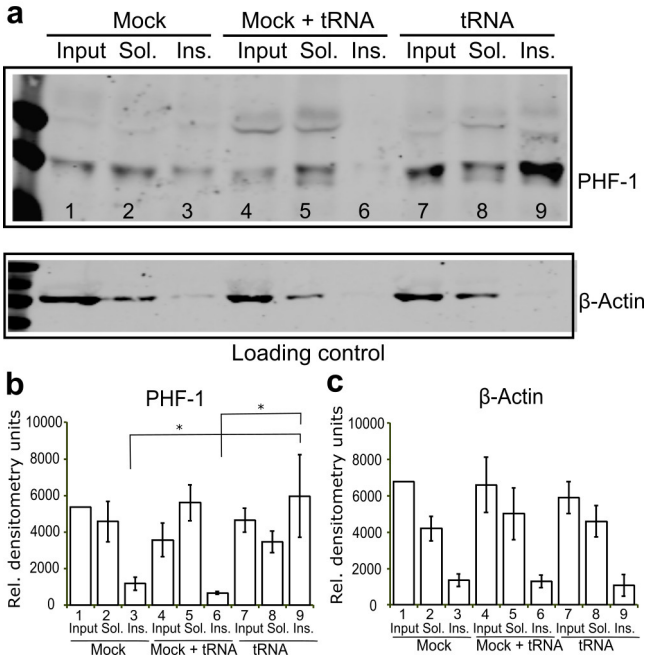

645

646 **Fig. 5: tRNA transfection accumulates sarkosyl insoluble Tau in hiPSC derived neurons.** (a)

647 Cells transfected with tRNA but not cells transfected in the absence of nucleic acids (Mock, lane

648 3) present an evident accumulation of sarkosyl insoluble Tau (tRNA, lane 9). Addition of tRNA

649 to the lysis buffer is insufficient to increase the Tau present in the insoluble fractions (Mock +

650 tRNA, lane 6). (b-c) Quantification of PHF-1 Tau (b) and β-actin (c) level are shown. Error bar

651 represents standard error of the mean. * $p < 0.05$, n=5.

652

References

1. Goedert M, Jakes R, Spillantini MG, Hasegawa M, Smith MJ, Crowther RA. Assembly of microtubule-associated protein tau into Alzheimer-like filaments induced by sulphated glycosaminoglycans. Nature. 1996;383(6600):550-3.
2. Kampers T, Friedhoff P, Biernat J, Mandelkow EM, Mandelkow E. RNA stimulates aggregation of microtubule-associated protein tau into Alzheimer-like paired helical filaments. FEBS Letters. 1996;399(3):344-9. doi: http://dx.doi.org/10.1016/S0014-5793(96)01386-5.
3. Wang X, Wang D, Zhao J, Qu M, Zhou X, He H, et al. The Proline-Rich Domain and the Microtubule Binding Domain of Protein Tau acting as RNA Binding Domains. Protein & Peptide Letters. 2006;13:679-85.
4. Sanders David W, Kaufman Sarah K, DeVos Sarah L, Sharma Apurwa M, Mirbaha H, Li A, et al. Distinct Tau Prion Strains Propagate in Cells and Mice and Define Different Tauopathies. Neuron. 2014;82(6):1271-88. doi: http://dx.doi.org/10.1016/j.neuron.2014.04.047.
5. Goedert M. Alzheimer's and Parkinson's diseases: The prion concept in relation to assembled Aβ, tau, and α-synuclein. Science. 2015;349(6248):1255555. doi: 10.1126/science.1255555. PubMed PMID: 26250687.
6. Patel A, Lee Hyun O, Jawerth L, Maharana S, Jahnel M, Hein Marco Y, et al. A Liquid-to-Solid Phase Transition of the ALS Protein FUS Accelerated by Disease Mutation. Cell. 2015;162(5):1066-77. doi: 10.1016/j.cell.2015.07.047.
7. Kato M, Han TW, Xie S, Shi K, Du X, Wu LC, et al. Cell-free formation of RNA granules: Low complexity sequence domains form dynamic fibers within hydrogels. Cell. 2012;149(4):753-67. doi: 10.1016/j.cell.2012.04.017.
8. Lee K-H, Zhang P, Kim Hong J, Mitrea DM, Sarkar M, Freibaum BD, et al. C9orf72 Dipeptide Repeats Impair the Assembly, Dynamics, and Function of Membrane-Less Organelles. Cell. 2016;167(3):774-88.e17. doi: http://dx.doi.org/10.1016/j.cell.2016.10.002.
9. Lin Y, Mori E, Kato M, Xiang S, Wu L, Kwon I, et al. Toxic PR Poly-Dipeptides Encoded by the C9orf72 Repeat Expansion Target LC Domain Polymers. Cell. 2016;167(3):789-802.e12. doi: http://dx.doi.org/10.1016/j.cell.2016.10.003.
10. Molliex A, Temirov J, Lee J, Coughlin M, Kanagaraj Anderson P, Kim Hong J, et al. Phase Separation by Low Complexity Domains Promotes Stress Granule Assembly and Drives Pathological Fibrillization. Cell. 2015;163(1):123-33. doi: http://dx.doi.org/10.1016/j.cell.2015.09.015.
11. Kim HJ, Kim NC, Wang YD, Scarborough EA, Moore J, Diaz Z, et al. Mutations in prion-like domains in hnRNPA2B1 and hnRNPA1 cause multisystem proteinopathy and ALS. Nature. 2013;495(7442):467-73. doi: 10.1038/nature11922.
12. Pak Chi W, Kosno M, Holehouse Alex S, Padrick Shae B, Mittal A, Ali R, et al. Sequence Determinants of Intracellular Phase Separation by Complex Coacervation of a Disordered Protein. Molecular Cell. 2016;63(1):72-85. doi: http://dx.doi.org/10.1016/j.molcel.2016.05.042.
13. Jho Y, Yoo HY, Lin Y, Han S, Hwang DS. Molecular and structural basis of low interfacial energy of complex coacervates in water. Advances in Colloid and Interface Science. 2016. doi: http://dx.doi.org/10.1016/j.cis.2016.07.003.

14. Huang K-Y, Yoo HY, Jho Y, Han S, Hwang DS. Bicontinuous Fluid Structure with Low Cohesive Energy: Molecular Basis for Exceptionally Low Interfacial Tension of Complex Coacervate Fluids. ACS Nano. 2016;10(5):5051-62. doi: 10.1021/acsnano.5b07787.

15. Bungenberg de Jong HG. Colloid Science. In: Kruyt HR, editor. II. Amsterdam: Elsevier Publishing Co. Inc; 1949. p. 335-432.

16. Hwang DS, Zeng H, Srivastava A, Krogstad DV, Tirrell M, Israelachvili JN, et al. Viscosity and interfacial properties in a mussel-inspired adhesive coacervate. Soft Matter. 2010;6(14):3232-6. doi: 10.1039/C002632H.

17. Overbeek JT, Voorn MJ. Phase separation in polyelectrolyte solutions; theory of complex coacervation. J Cell Physiol Suppl. 1957;49(Suppl 1):7-22; discussion, -6. PubMed PMID: 13449108.

18. Dehmelt L, Halpain S. The MAP2/Tau family of microtubule-associated proteins. Genome Biol. 2005;6(1):204.

19. Friedersdorf M, Keene J. Advancing the functional utility of PAR-CLIP by quantifying background binding to mRNAs and lncRNAs. Genome Biology. 2014;15(1):R2.

20. Ryder SP, Recht MI, Williamson JR. Quantitative analysis of protein-RNA interactions by gel mobility shift. Methods in molecular biology (Clifton, NJ). 2008;488:99-115. doi: 10.1007/978-1-60327-475-3_7. PubMed PMID: PMC2928675.

21. Zucconi BE, Ballin JD, Brewer BY, Ross CR, Huang J, Toth EA, et al. Alternatively Expressed Domains of AU-rich Element RNA-binding Protein 1 (AUF1) Regulate RNA-binding Affinity, RNA-induced Protein Oligomerization, and the Local Conformation of Bound RNA Ligands. Journal of Biological Chemistry. 2010;285(50):39127-39.

22. Okunola HL, Krainer AR. Cooperative-Binding and Splicing-Repressive Properties of hnRNP A1. Molecular and Cellular Biology. 2009;29(20):5620-31.

23. Aumiller WM, Pir-Cakmak F, Davis BW, Keating CD. RNA-based coacervates as a model for membraneless organelles: Formation, properties, and interfacial liposome assembly. Langmuir. 2016. doi: 10.1021/acs.langmuir.6b02499.

24. Ortony JH, Hwang DS, Franck JM, Waite JH, Han S. Asymmetric Collapse in Biomimetic Complex Coacervates Revealed by Local Polymer and Water Dynamics. Biomacromolecules. 2013;14(5):1395-402. doi: 10.1021/bm4000579.

25. Pérez M, Valpuesta JM, Medina M, Montejo de Garcini E, Avila J. Polymerization of τ into Filaments in the Presence of Heparin: The Minimal Sequence Required for τ - τ Interaction. Journal of Neurochemistry. 1996;67(3):1183-90. doi: 10.1046/j.1471-4159.1996.67031183.x.

26. von Bergen M, Barghorn S, Biernat J, Mandelkow E-M, Mandelkow E. Tau aggregation is driven by a transition from random coil to beta sheet structure. Biochimica et Biophysica Acta (BBA) - Molecular Basis of Disease. 2005;1739(2–3):158-66. doi: http://dx.doi.org/10.1016/j.bbadis.2004.09.010.

27. Qin J, Priftis D, Farina R, Perry SL, Leon L, Whitmer J, et al. Interfacial Tension of Polyelectrolyte Complex Coacervate Phases. ACS Macro Letters. 2014;3(6):565-8. doi: 10.1021/mz500190w.

28. Priftis D, Megley K, Laugel N, Tirrell M. Complex coacervation of poly(ethylene-imine)/polypeptide aqueous solutions: Thermodynamic and rheological characterization. Journal of Colloid and Interface Science. 2013;398:39-50. doi: http://dx.doi.org/10.1016/j.jcis.2013.01.055.

739 29. Aberkane L, Jasniewski J, Gaiani C, Scher J, Sanchez C. Thermodynamic
740 Characterization of Acacia Gum−β-Lactoglobulin Complex Coacervation. Langmuir.
741 2010;26(15):12523-33. doi: 10.1021/la100705d.
742 30. Xu AY, Melton LD, Jameson GB, Williams MAK, McGillivray DJ. Structural
743 mechanism of complex assemblies: characterisation of beta-lactoglobulin and pectin interactions.
744 Soft Matter. 2015;11(34):6790-9. doi: 10.1039/C5SM01378J.
745 31. Wolde PRt, Frenkel D. Enhancement of Protein Crystal Nucleation by Critical Density
746 Fluctuations. Science. 1997;277(5334):1975.
747 32. Takahashi K, Yamanaka S. Induction of Pluripotent Stem Cells from Mouse Embryonic
748 and Adult Fibroblast Cultures by Defined Factors. Cell. 126(4):663-76. doi:
749 10.1016/j.cell.2006.07.024.
750 33. Coppola G, Chinnathambi S, Lee JJ, Dombroski BA, Baker MC, Soto-Ortolaza AI, et al.
751 Evidence for a role of the rare p.A152T variant in MAPT in increasing the risk for FTD-
752 spectrum and Alzheimer's diseases. Human Molecular Genetics. 2012;21(15):3500-12.
753 34. Fong H, Wang C, Knoferle J, Walker D, Balestra Maureen E, Tong Leslie M, et al.
754 Genetic Correction of Tauopathy Phenotypes in Neurons Derived from Human Induced
755 Pluripotent Stem Cells. Stem Cell Reports. 2013;1(3):226-34. doi: 10.1016/j.stemcr.2013.08.001.
756 PubMed PMID: PMC3849235.
757 35. Mak SK, Huang YA, Iranmanesh S, Vangipuram M, Sundararajan R, Nguyen L, et al.
758 Small molecules greatly improve conversion of human-induced pluripotent stem cells to the
759 neuronal lineage. Stem Cells Int. 2012;2012:140427. doi: 10.1155/2012/140427. PubMed PMID:
760 22567022; PubMed Central PMCID: PMCPMC3339118.
761 36. Huppertz I, Attig J, D'Ambrogio A, Easton LE, Sibley CR, Sugimoto Y, et al. iCLIP:
762 Protein–RNA interactions at nucleotide resolution. Methods. 2014;65(3):274-87. doi:
763 http://dx.doi.org/10.1016/j.ymeth.2013.10.011.
764 37. Tollervey JR, Curk T, Rogelj B, Briese M, Cereda M, Kayikci M, et al. Characterizing
765 the RNA targets and position-dependent splicing regulation by TDP-43. Nat Neurosci.
766 2011;14(4):452-8. doi:
767 http://www.nature.com/neuro/journal/v14/n4/abs/nn.2778.html#supplementary-information.
768 38. Hafner M, Landthaler M, Burger L, Khorshid M, Hausser J, Berninger P, et al.
769 Transcriptome-wide identification of RNA-binding protein and microRNA target sites by PAR-
770 CLIP. Cell. 2010;141(1):129-41. doi: 10.1016/j.cell.2010.03.009. PubMed PMID: 20371350;
771 PubMed Central PMCID: PMC2861495.
772 39. Yanamandra K, Kfoury N, Jiang H, Mahan TE, Ma S, Maloney SE, et al. Anti-tau
773 antibodies that block tau aggregate seeding in vitro markedly decrease pathology and improve
774 cognition in vivo. Neuron. 2013;80(2):402-14. doi: 10.1016/j.neuron.2013.07.046. PubMed
775 PMID: PMC3924573.
776 40. Martin M. Cutadapt removes adapter sequences from high-throughput sequencing reads.
777 EMBnet journal. 2011;17(1):10-2.
778 41. Langmead B, Salzberg SL. Fast gapped-read alignment with Bowtie 2. Nat Meth.
779 2012;9(4):357-9. doi: 10.1038/nmeth.1923
780 http://www.nature.com/nmeth/journal/v9/n4/abs/nmeth.1923.html#supplementary-information.
781 42. Wang L, Wang S, Li W. RSeQC: quality control of RNA-seq experiments.
782 Bioinformatics. 2012;28(16):2184-5. doi: 10.1093/bioinformatics/bts356.

783 43. Althammer S, González-Vallinas J, Ballaré C, Beato M, Eyras E. Pyicos: a versatile
784 toolkit for the analysis of high-throughput sequencing data. Bioinformatics. 2011;27(24):3333-
785 40.
786 44. Konig J, Zarnack K, Rot G, Curk T, Kayikci M, Zupan B, et al. iCLIP reveals the
787 function of hnRNP particles in splicing at individual nucleotide resolution. Nat Struct Mol Biol.
788 2010;17(7):909-15. doi:
789 http://www.nature.com/nsmb/journal/v17/n7/abs/nsmb.1838.html#supplementary-information.
790 45. Langmead B, Trapnell C, Pop M, Salzberg S. Ultrafast and memory-efficient alignment
791 of short DNA sequences to the human genome. Genome Biology. 2009;10(3):R25.
792 46. Fasman GD, editor. Handbook of Biochemistry and Molecular Biology. 3rd ed.
793 Cleveland, OH.: CRC Press; 1976.
794 47. Jeschke G, Chechik V, Ionita P, Godt A, Zimmermann H, Banham J, et al.
795 DeerAnalysis2006—a comprehensive software package for analyzing pulsed ELDOR data.
796 Applied Magnetic Resonance. 2006;30(3):473-98. doi: 10.1007/BF03166213.
797 48. DeTure M, Ko L-w, Easson C, Yen S-H. tau Assembly in Inducible Transfectants
798 Expressing Wild-Type or FTDP-17 tau. The American Journal of Pathology. 2002;161(5):1711-
799 22. PubMed PMID: PMC1850799.
800 49. Carrettiero DC, Hernandez I, Neveu P, Papagiannakopoulos T, Kosik KS. The Co-
801 chaperone BAG2 Sweeps PHF Insoluble Tau from the Microtubule. Journal of Neuroscience.
802 2009;29(7):2151-61. doi: 10.1523/JNEUROSCI.4660-08.2009. PubMed PMID: PMC2768429.

803